Supporting information

Exploring the physicochemical role of Pd dopant in promoting Li-ion diffusion dynamics and storage performance for NbS_2 at atomic scale

Piaopiao Wen[a], Huangkai Wang[a], Xianyou Wang[b], Haibo Wang[c,*], Yansong Bai[b,*], Zhenhua Yang[a,*]

[a]*Key Laboratory of Low Dimensional Materials & Application Technology of Ministry of Education, School of Materials Science and Engineering, Xiangtan University, Xiangtan 411105, Hunan, China*

[b]*National Base for International Science & Technology Cooperation, National-Local Joint Engineering Laboratory for Key Materials of New Energy Storage Battery, Hunan Province Key Laboratory of Electrochemical Energy Storage and Conversion, School of Chemistry, Xiangtan University, Xiangtan 411105, Hunan, China.*

[c]*NanChang JiaoTong Institute, Nanchang 330100, Jiangxi, China*

[*]Corresponding authors. Address: *Key Laboratory of Low Dimensional Materials & Application Technology of Ministry of Education, School of Materials Science and Engineering, Xiangtan University, Xiangtan 411105, Hunan, China*.
E-mail address: yangzhenhua@xtu.edu.cn (Zhenhua Yang)
whbcsu@ncjti.edu.cn(Haibo Wang)
baiyansong2007@126.com (Yansong Bai)

1. Structural properties

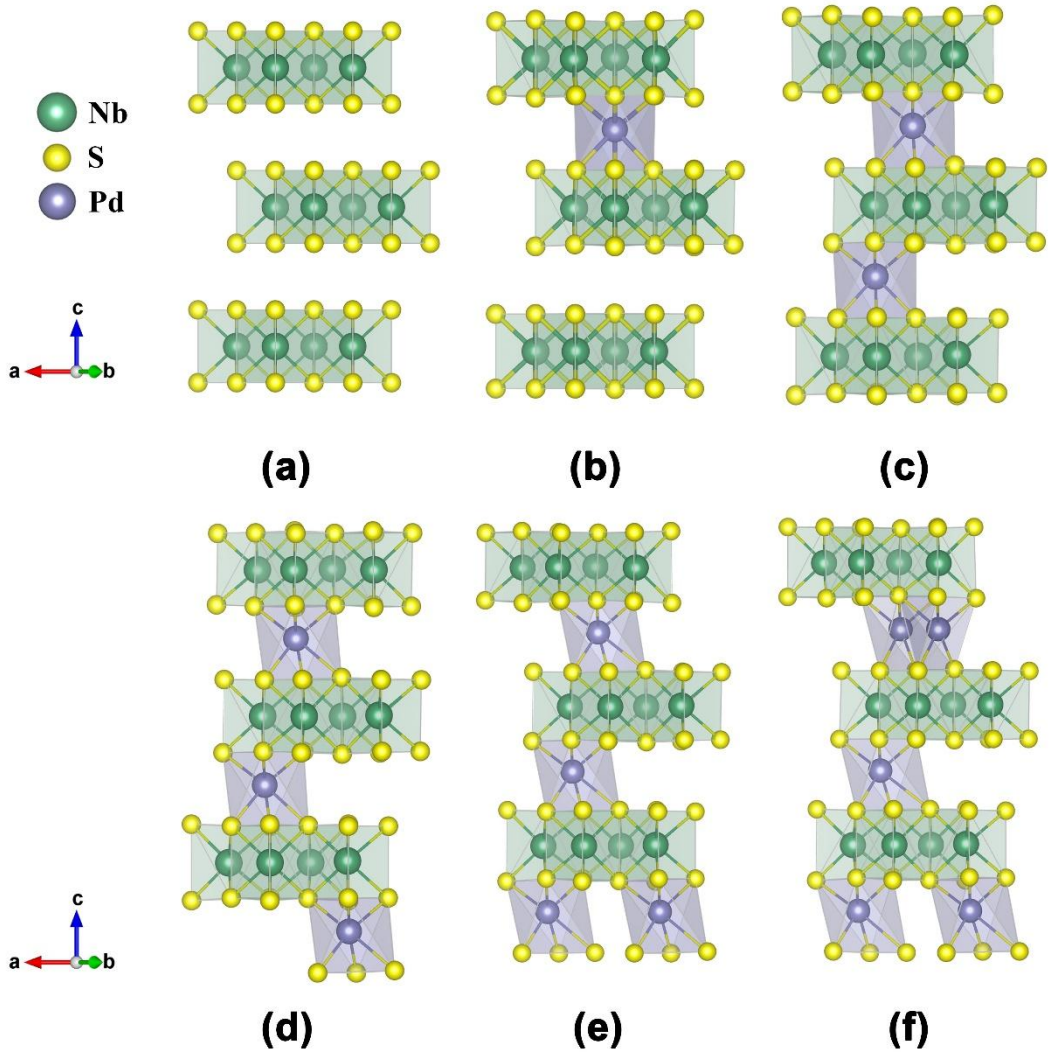

Fig. S1 The crystal structures of (a) NbS_2, (b) $Pd_{0.083}NbS_2$, (c) $Pd_{0.167}NbS_2$, (d) $Pd_{0.25}NbS_2$, (e) $Pd_{0.333}NbS_2$, and (f) $Pd_{0.417}NbS_2$.

2. Screening the structure of Pd_xNbS_2 (x = 0, 0.083, 0.167, 0.250, 0.333, 0.417)

Three kinds of Pd intercalation sites were considered: an octahedral site (directly above the Nb atom) and two tetrahedral sites (one where Pd is directly above the S atom, and the other where Pd is directly below the S atom). (see Fig. S2). Based on the first-principle calculation, the Pd atom is favorable to occupy the octahedral interstice. The Pd-S bond lengths vary from 2.42 Å to 2.53 Å, which is close to the range of ionic and covalent bonds of Pd-S (see Fig. S2(a)). Weak orbital hybridization between Pd-4d orbitals and surrounding S-3p orbitals is observed, indicating that there is a weak covalent interaction between Pd and S.

Furthermore, in order to determine which kind of doping for Pd it is in the crystal structure of NbS_2 (embedded type or substitution type), the formation energy of Pd_xNbS_2 and $Pd_xNb_{(1-x)}S_2$ (*i.e.*, $NbPd_3$, Pd_4S, Pd_3S, PdS_2, PdS, $Pd_{16}S_7$, Nb_2PdS_5, and Nb_2PdS_6) were also calculated. Fig. S8 and S9 show the formation energy of Pd_xNbS_2 and $Pd_xNb_{(1-x)}S_2$ under the growth condition of A-B. It can be easily found that no matter what kind of doping system it is for Pd element, the formation energy of the embedded type is lower than that of the substituted type. So, the Pd doping in the phase of NbS_2 compound is preferentially embedded in the van der Waals interstice.

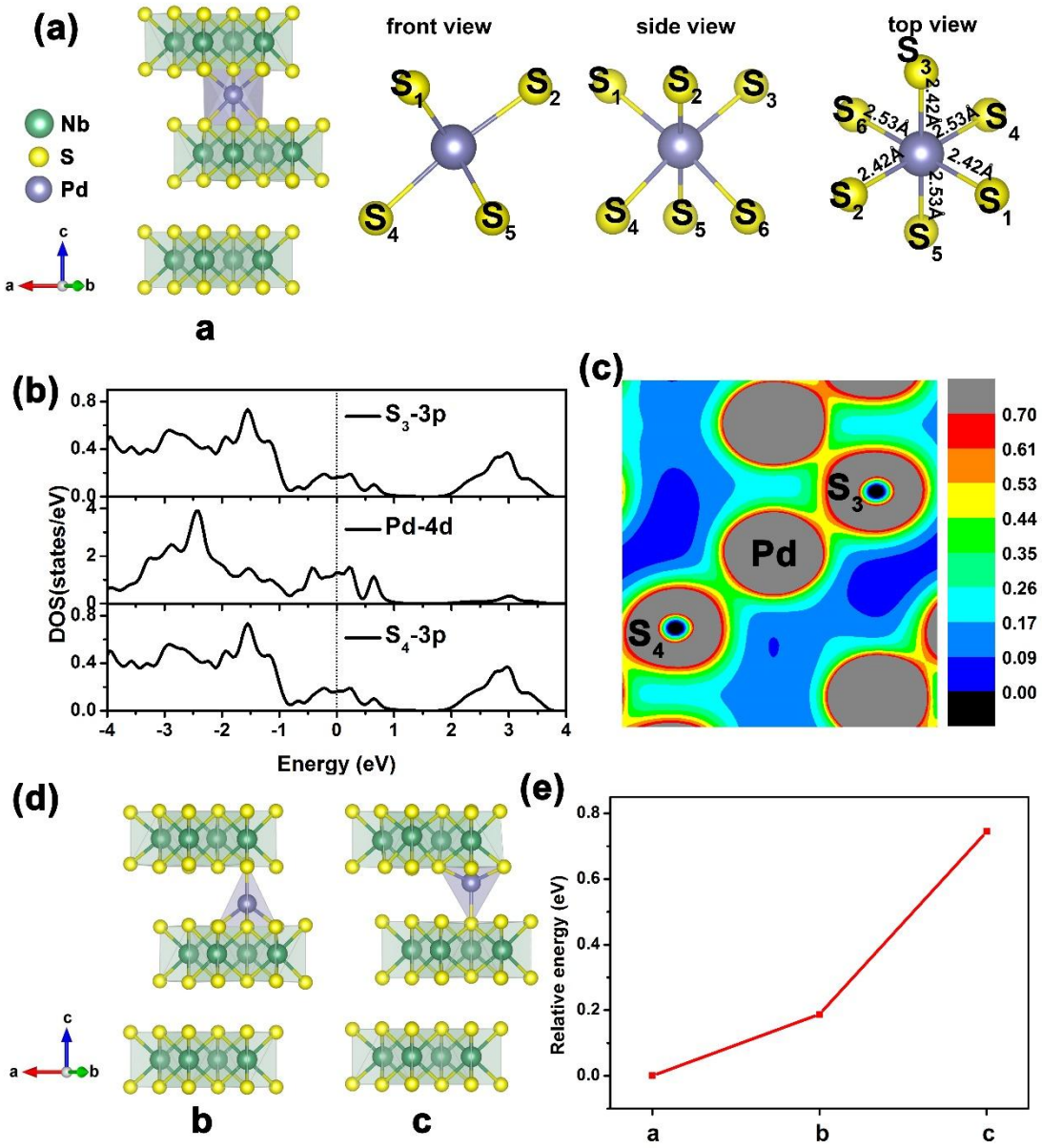

Fig. S2 Three different Pd doping sites. (a) octahedral site, (d) two different tetrahedral sites. (b) The density of states (DOS) and (c) charge density of S_3-Pd-S_4 clusters when Pd occupies the octahedral site. (e) the relative energies as a function of Pd doping sites.

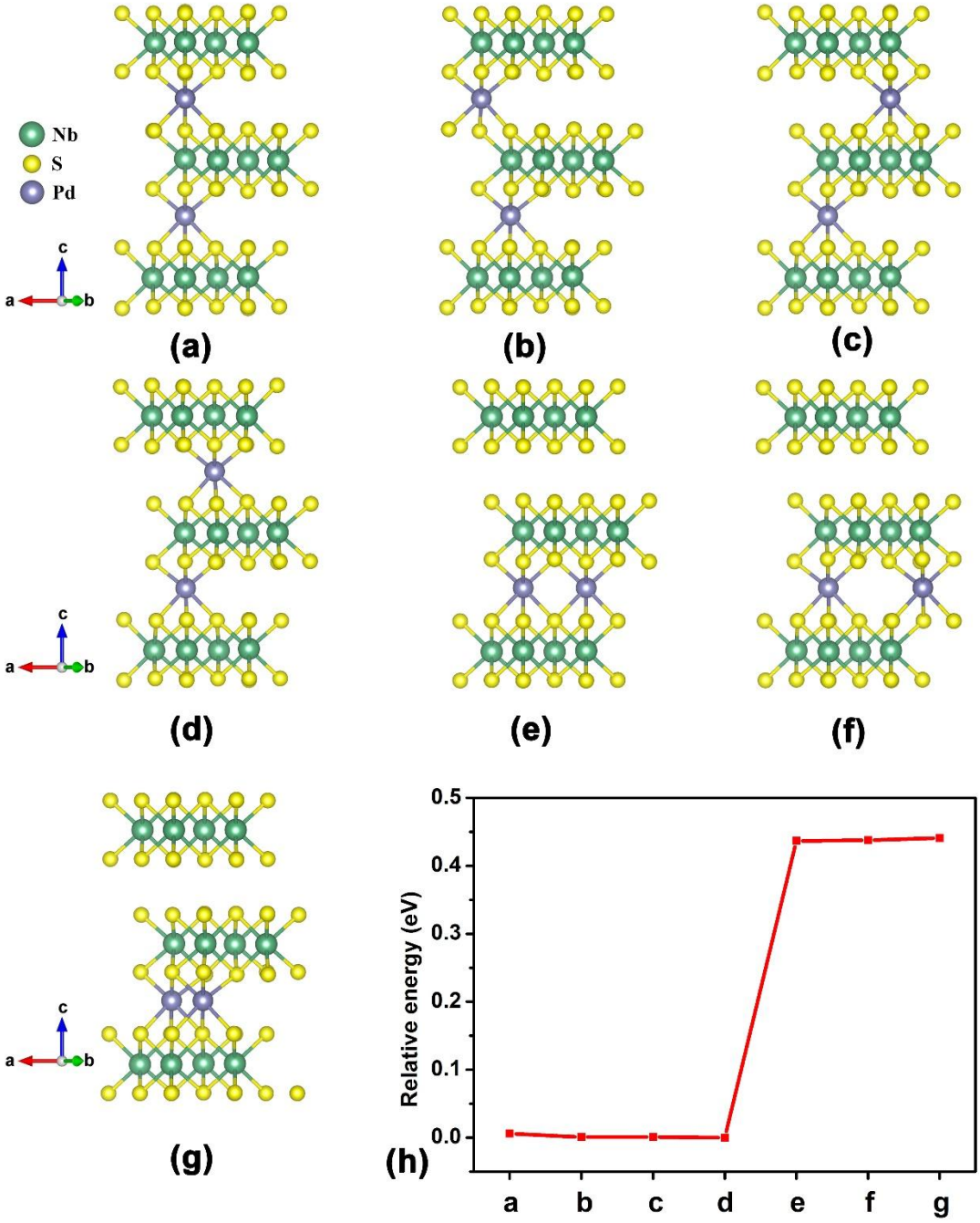

Fig. S3 Seven kinds of structures of $Pd_{0.167}NbS_2$ and (h) their corresponding relative energies. Different Pd-doped structures are labeled as (a), (b), (c), (d), (e) and (g).

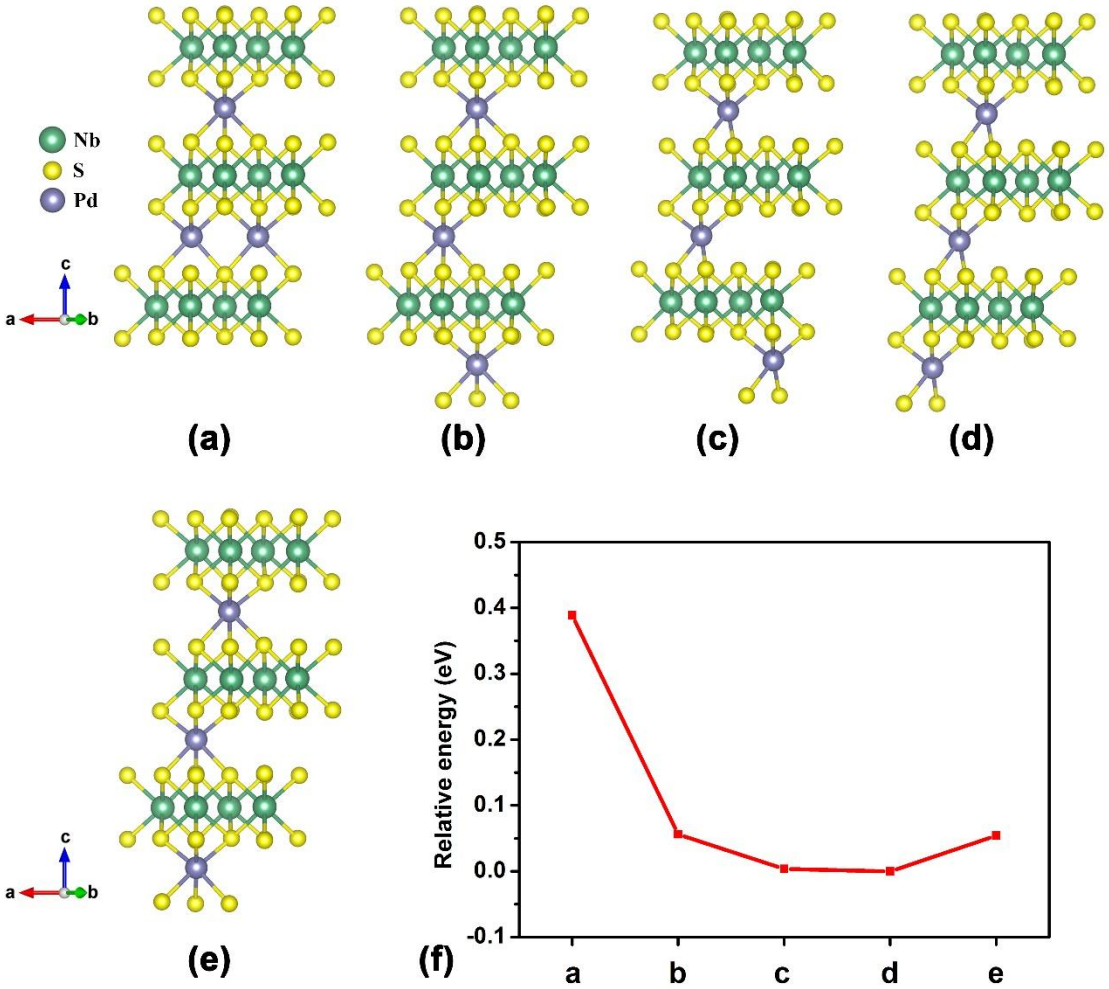

Fig. S4 Five kinds of structures of $Pd_{0.250}NbS_2$ and (f) their corresponding relative energies. Different Pd-doped structures are labeled as (a), (b), (c), (d) and (e).

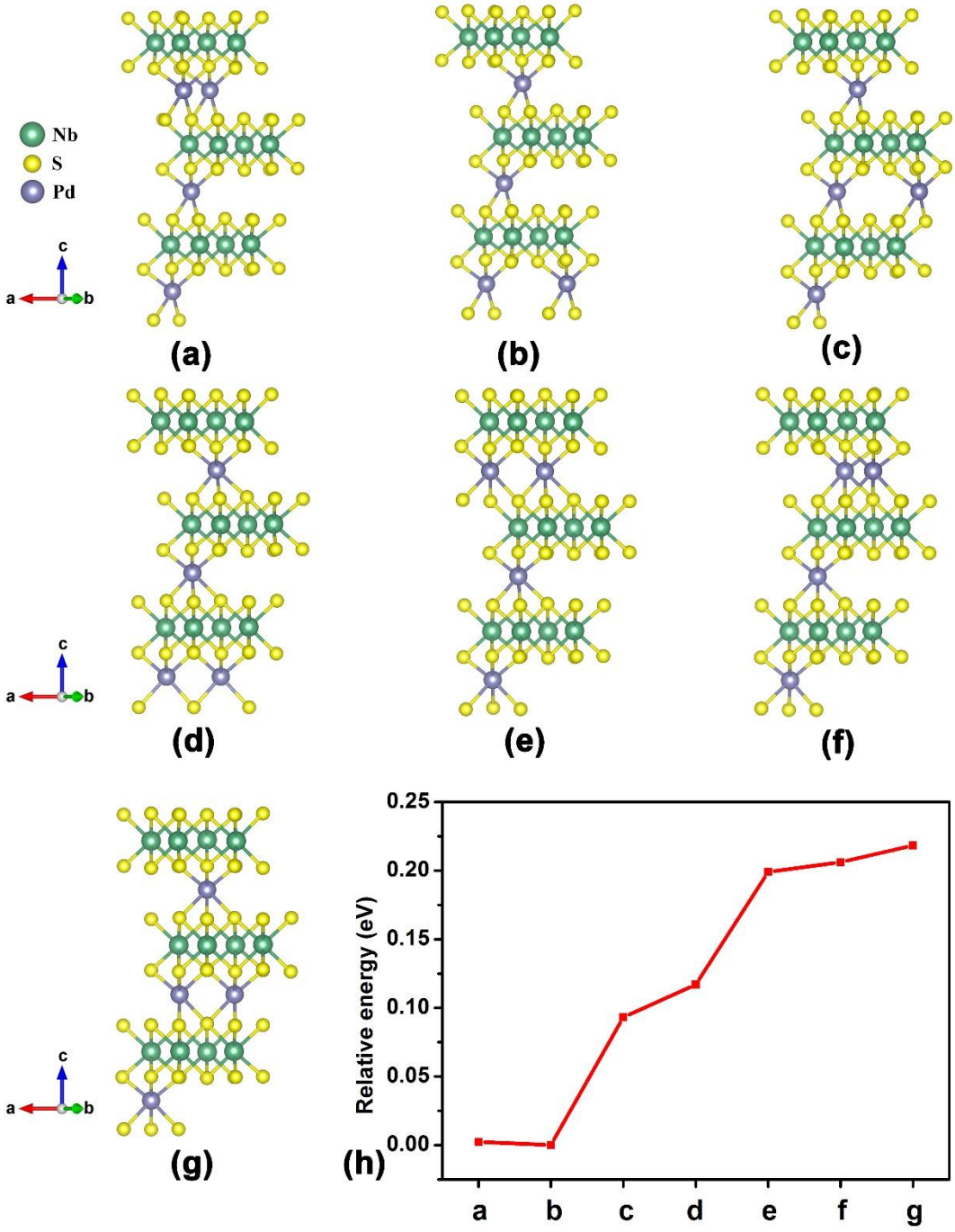

Fig. S5 Seven kinds of structures of $Pd_{0.333}NbS_2$ and (h) their corresponding relative energies. Different Pd-doped structures are labeled as (a), (b), (c), (d), (e) and (g).

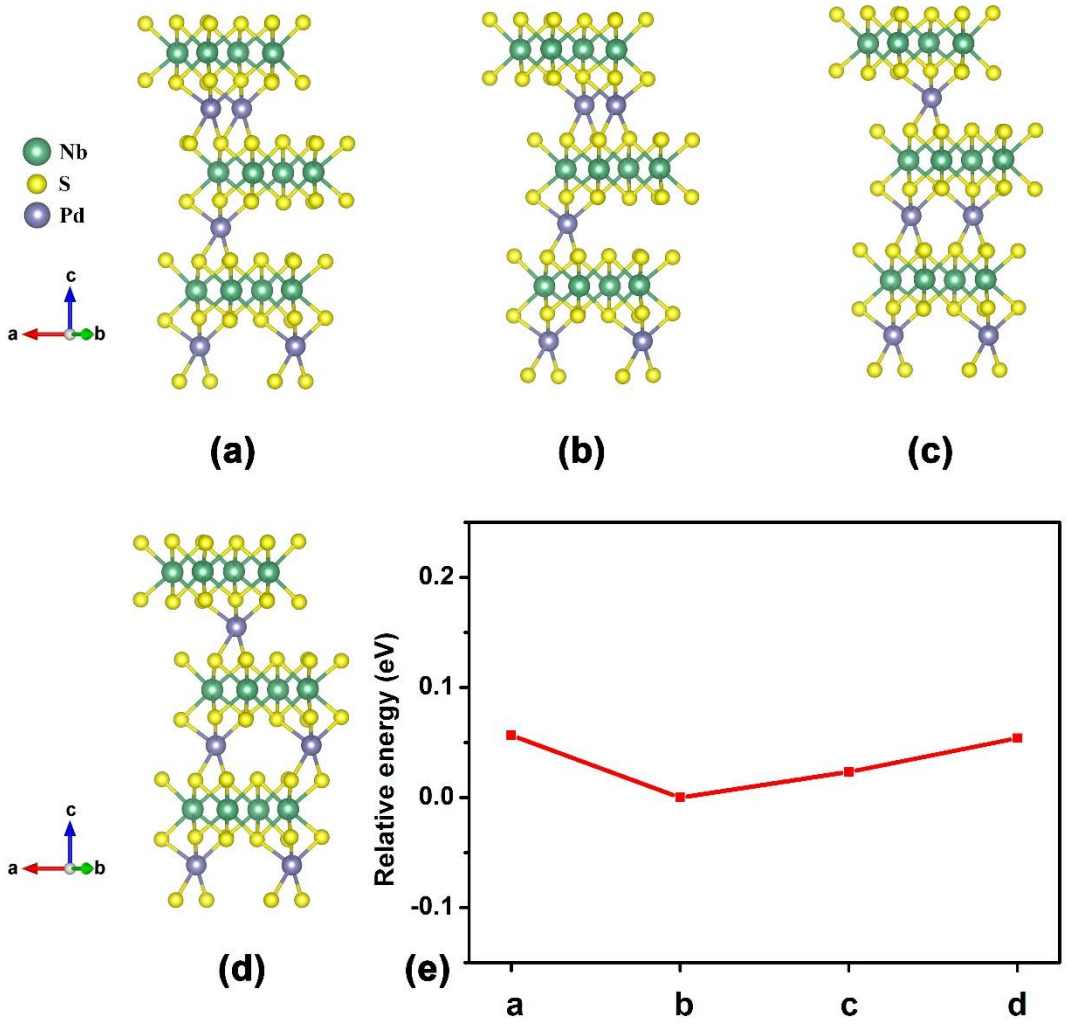

Fig. S6 Four kinds of structures of $Pd_{0.417}NbS_2$ and (e) their corresponding relative energies. Different Pd-doped structures are labeled as (a), (b), (c), and (d).

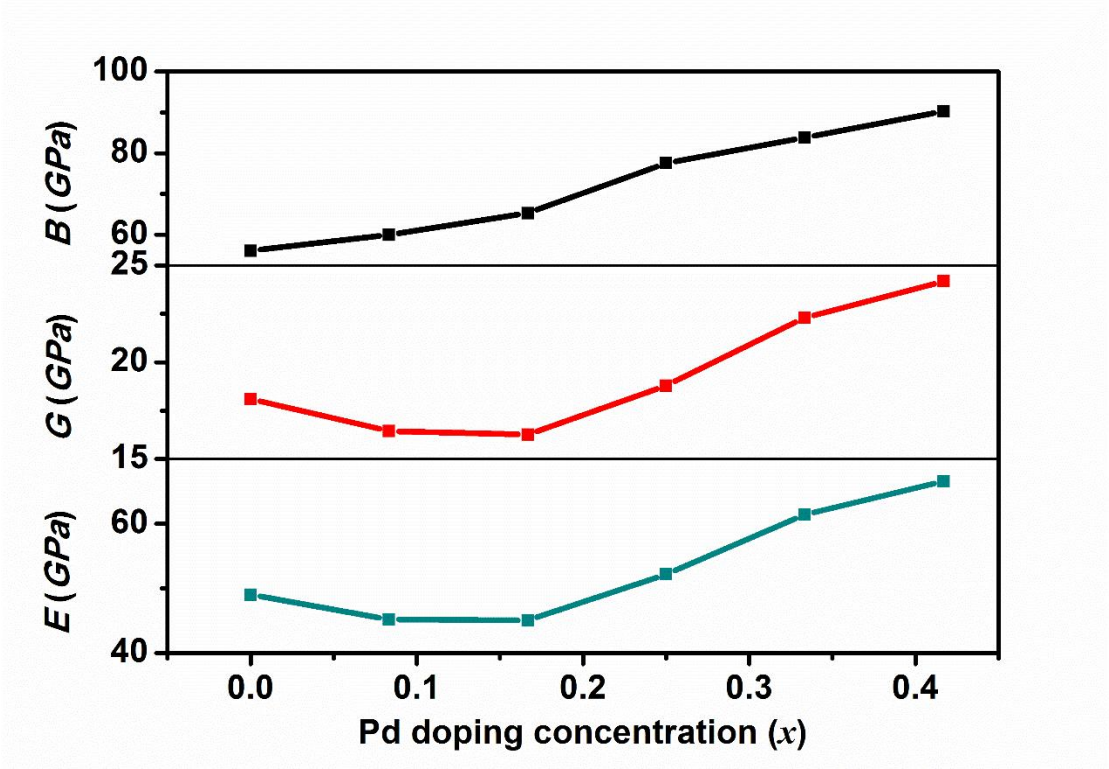

Fig. S7 The variation of *B*, *G* and *E* as a function of Pd-doped concentration (*x*) for Pd_xNbS_2 (*x* = 0, 0.083, 0.167, 0.250, 0.333, 0.417).

To evaluate the stability of the heteroatom-doped structure, the impurity formation energy of $Pd_{1-x}NbS_2$ is calculated as the following formula:[1]

$$E_{form} = E_{tot}(Pd_xNb_{1-x}S_2) - E_{tot}(NbS_2) - \sum n_i(\Delta\mu_i + \mu_i) \quad (1)$$

Where the $E_{tot}(Pd_xNb_{1-x}S_2)$ represents the total energy of the $Pd_xNb_{1-x}S_2$, and the $E_{tot}(NbS_2)$ is the total energy of the perfect crystal cell. n_i is the number of atoms (add: n_i <0, remove: n_i >0). μ_i is the chemical potential of the host atoms or the impurity atoms. $\Delta\mu_i$ is the relative chemical potential of element *i* under different chemical growth environments. μ_{Nb}, μ_S and μ_{Pd} refer to the total energies of Nb, S, and Pd elemental solids, respectively.

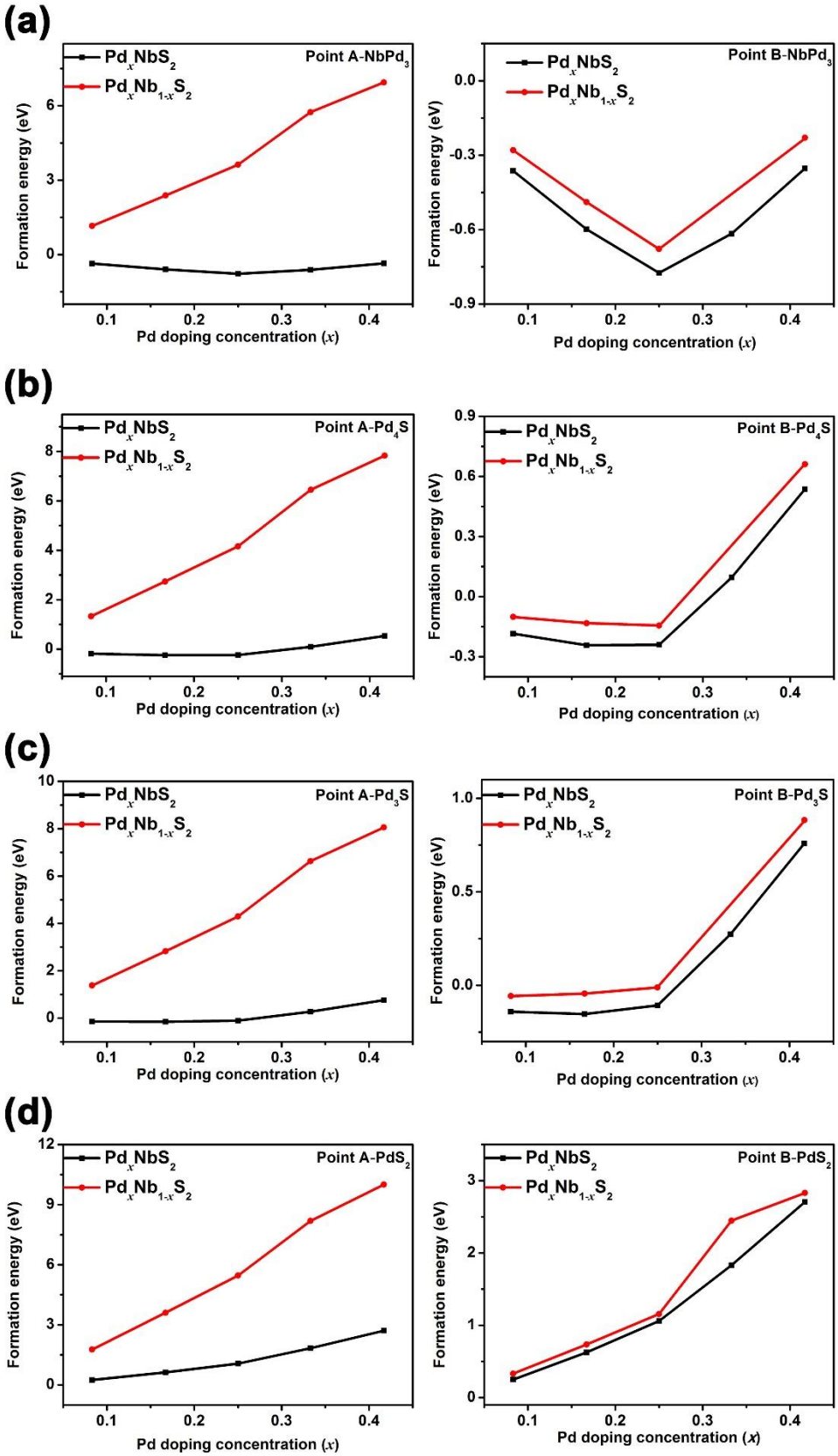

Fig. S8 The formation energies of (a) $NbPd_3$, (b) Pd_4S, (c) Pd_3S and (d) PdS_2 doping at the points A and B in the chemical potential region.

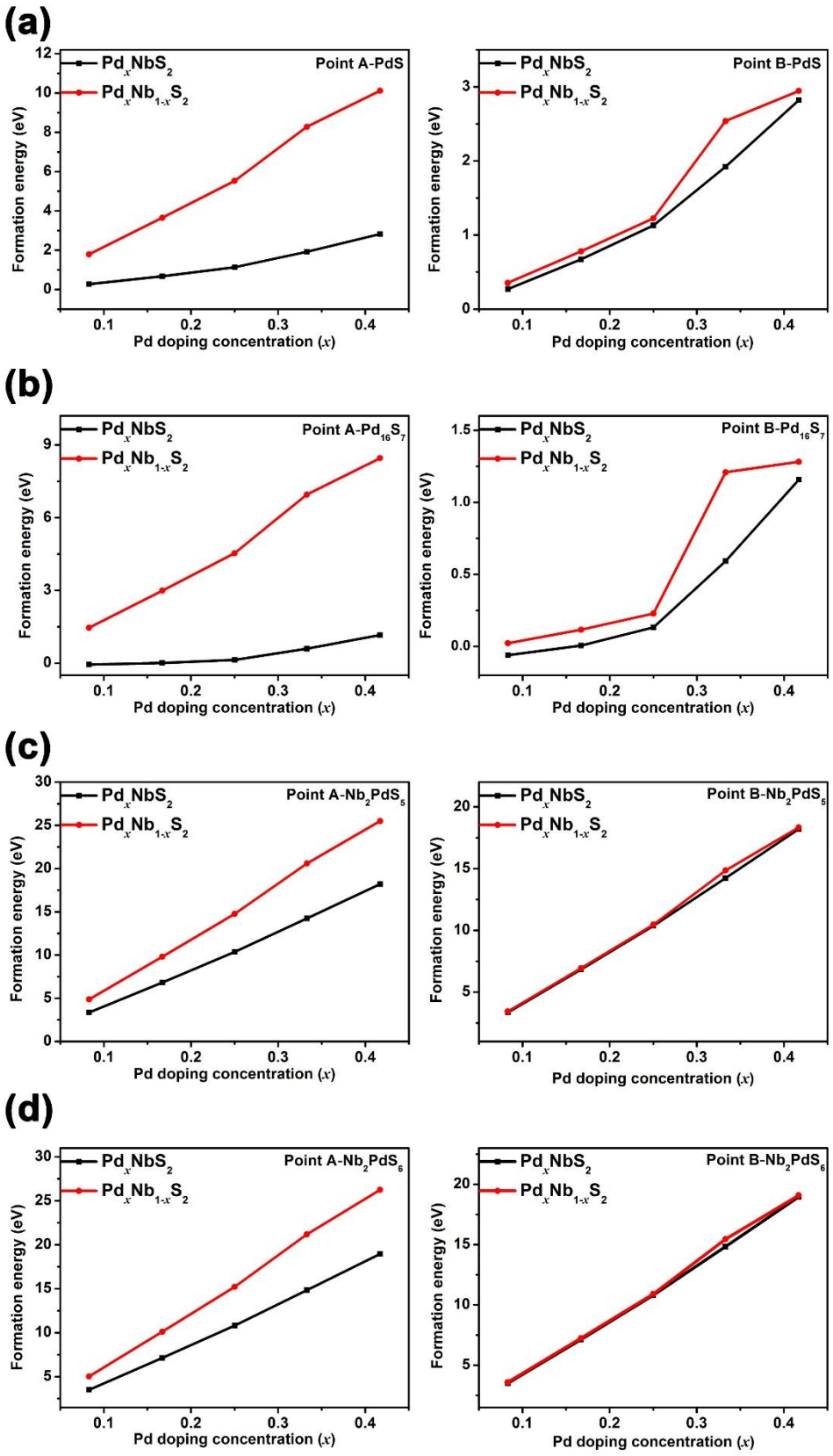

Fig. S9 The formation energies of (a) PdS, (b) $Pd_{16}S_7$, (c) Nb_2PdS_5, and (d) Nb_2PdS_6 doping at the points A and B in the chemical potential region.

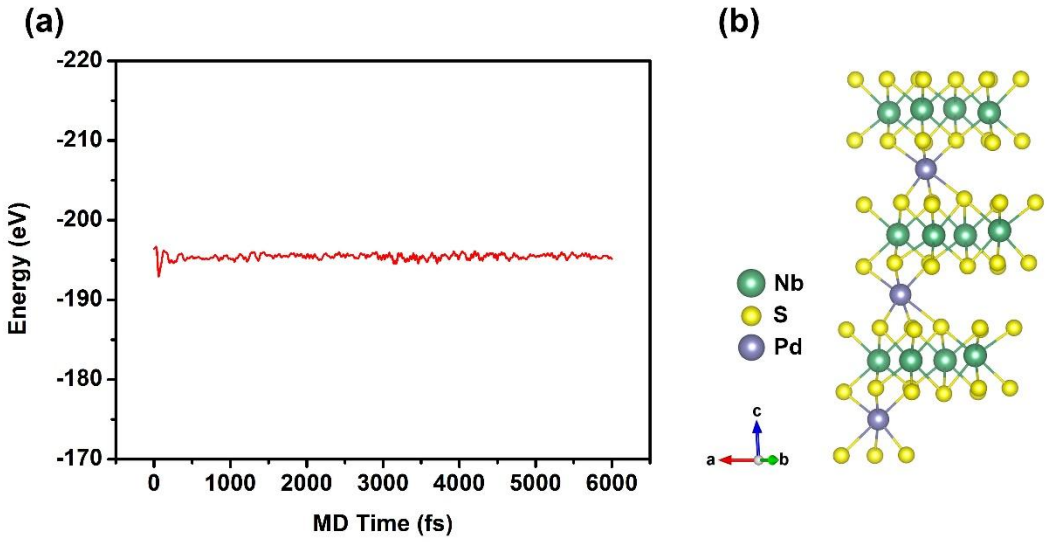

Fig. S10 (a) The total energies of $Pd_{0.25}NbS_2$ as a function of AIMD time. (b) The optimized structure of $Pd_{0.25}NbS_2$ at 300K after 6000 fs.

3. Electronic structure of Pd_xNbS_2 (x = 0, 0.083, 0.167, 0.250, 0.333, 0.417)

In order to consider the spin polarization of Pd metal, we have calculated the density of state (DOS) of Pd_xNbS_2 (0.083, 0.167, 0.250, 0.333, 0.417). It is noted that the spin-up and spin-down bands of Pd-4d and total DOS both show symmetric character (see Fig. S11). Therefore, Pd element in Pd_xNbS_2 (0.083, 0.167, 0.250, 0.333, 0.417) exhibits the character of non-spin polarization.

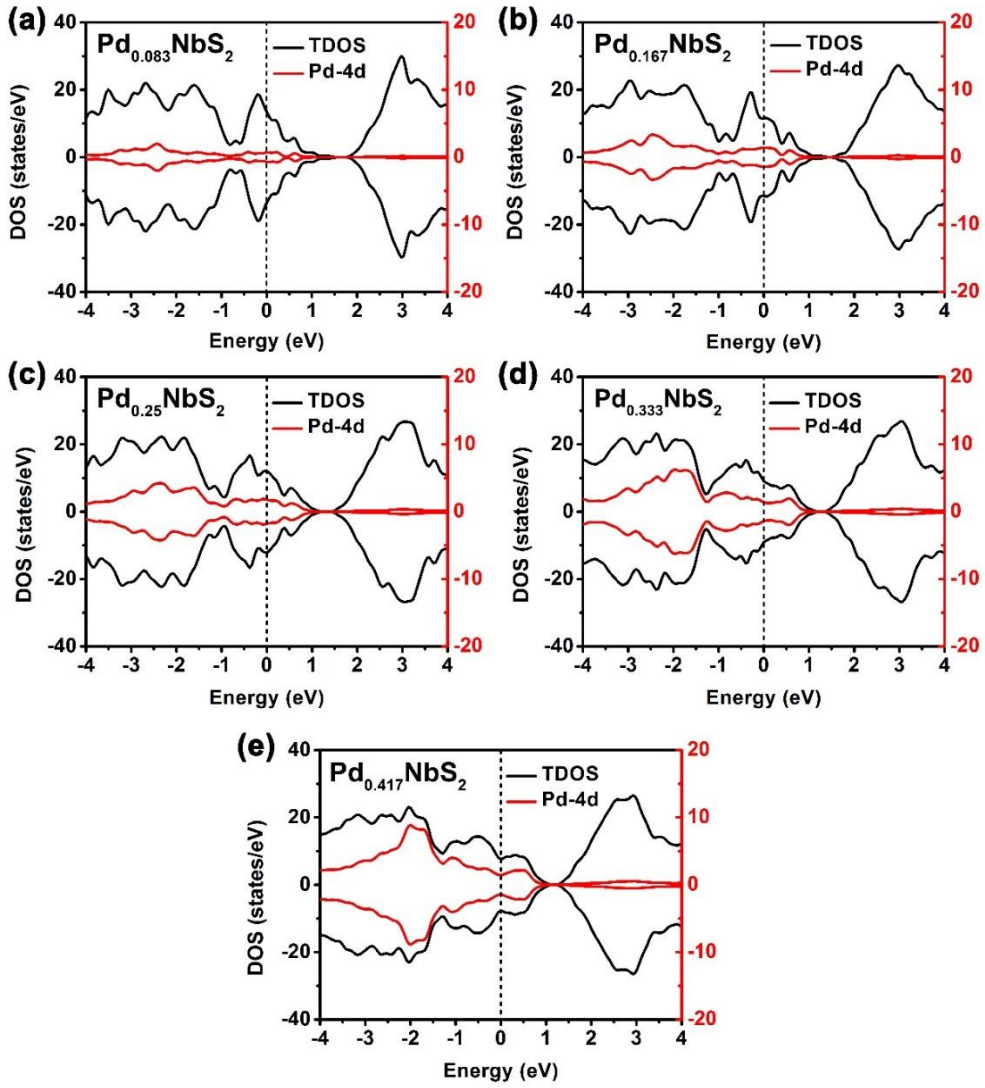

Fig. S11 The total DOS and partial DOS of Pd. (a) $Pd_{0.083}NbS_2$; (b)$Pd_{0.167}NbS_2$; (c) $Pd_{0.250}NbS_2$; (d) $Pd_{0.333}NbS_2$; (e)$Pd_{0.417}NbS_2$. The Fermi level is indicated by the dashed line.

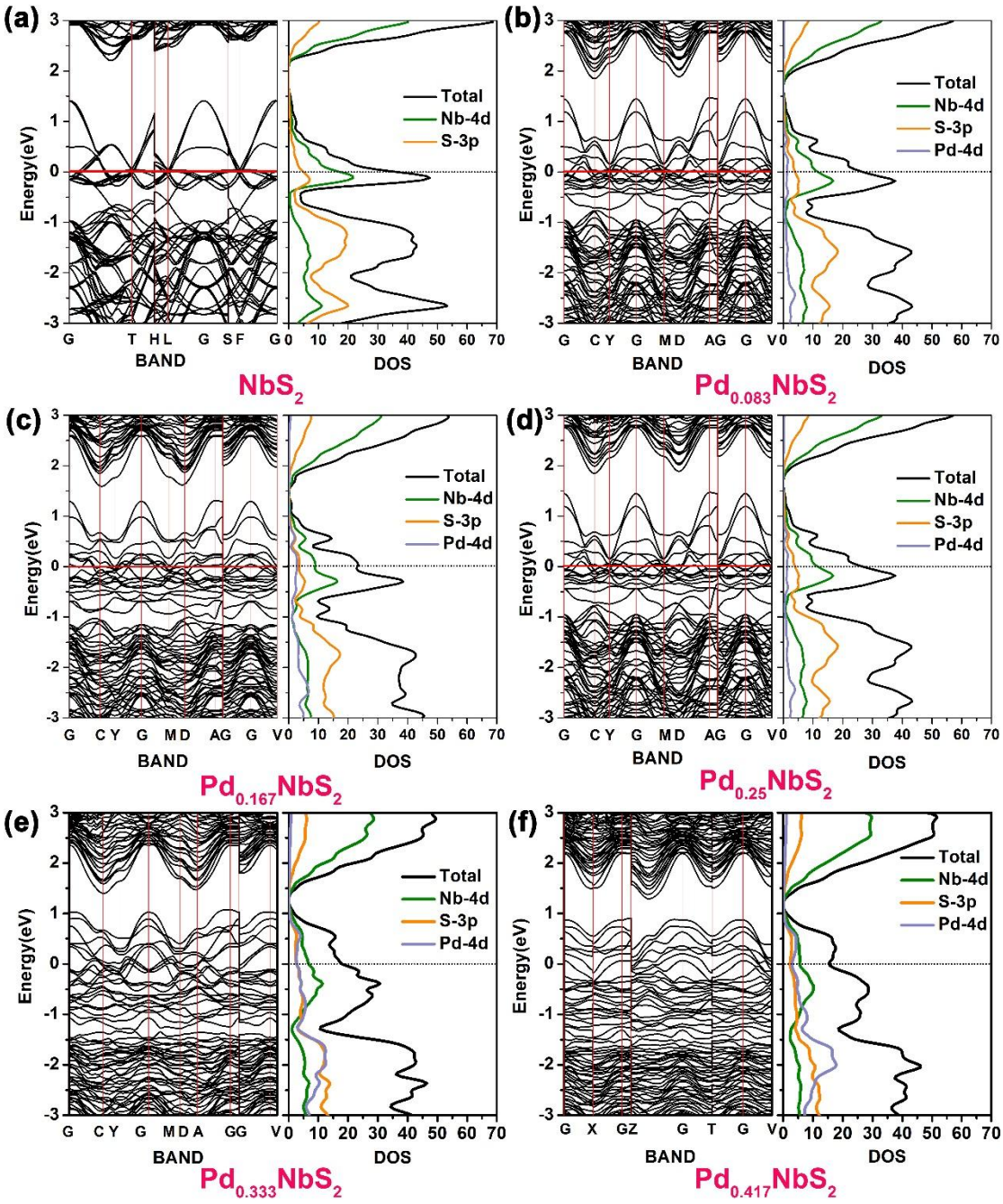

Fig. S12 Band structure and the density of states of (a) NbS_2, (b) $Pd_{0.083}NbS_2$, (c) $Pd_{0.167}NbS_2$, (d) $Pd_{0.25}NbS_2$, (e) $Pd_{0.333}NbS_2$, and (f) $Pd_{0.417}NbS_2$.

4. The Li insertion mechanism occurring in the Pd_xNbS_2 (x = 0, 0.083, 0.167, 0.250, 0.333, 0.417)

We introduced binding energy (E_{bind}) to evaluate the stability of the configuration of the embedded Li atoms and the binding energy can be defined as follows:[2, 3]

$$E_{bind} = E_{Li/Pd_xNbS_2} - E_{Pd_xNbS_2} - E_{Li} \quad (1)$$

where E_{Li/Pd_xNbS_2} and $E_{Pd_xNbS_2}$ are the total energy of Li/Pd_xNbS_2 and Pd_xNbS_2, respectively. E_{Li} is the energy per Li atom in the perfect crystal of Li. Firstly, we calculated the binding energy of Li atom in the $Pd_{0.083}NbS_2$ structure, as shown in Fig. S13. The binding energy of Li atom occupying the octahedral interstice position of site-1 is -2.50 eV. It is lower than that of the octahedral interstice position of two tetrahedrons (site-2 and site-3) and the octahedral interstice positions of site-4 which is located in the same layer doped by Pd. These results indicate that the Li atoms prefer to occupy the octahedral interstitial position of the Pd-free layer. Similarly, the binding energies of Li atoms in Pd_xNbS_2 structures at other concentrations were also calculated (for details, see Fig. S14-S17). The lowest binding energies of $Pd_{0.167}NbS_2$, $Pd_{0.25}NbS_2$, $Pd_{0.333}NbS_2$ and $Pd_{0.417}NbS_2$ are -2.53 eV, -2.21 eV, -2.16 eV and -2.12 eV, respectively.

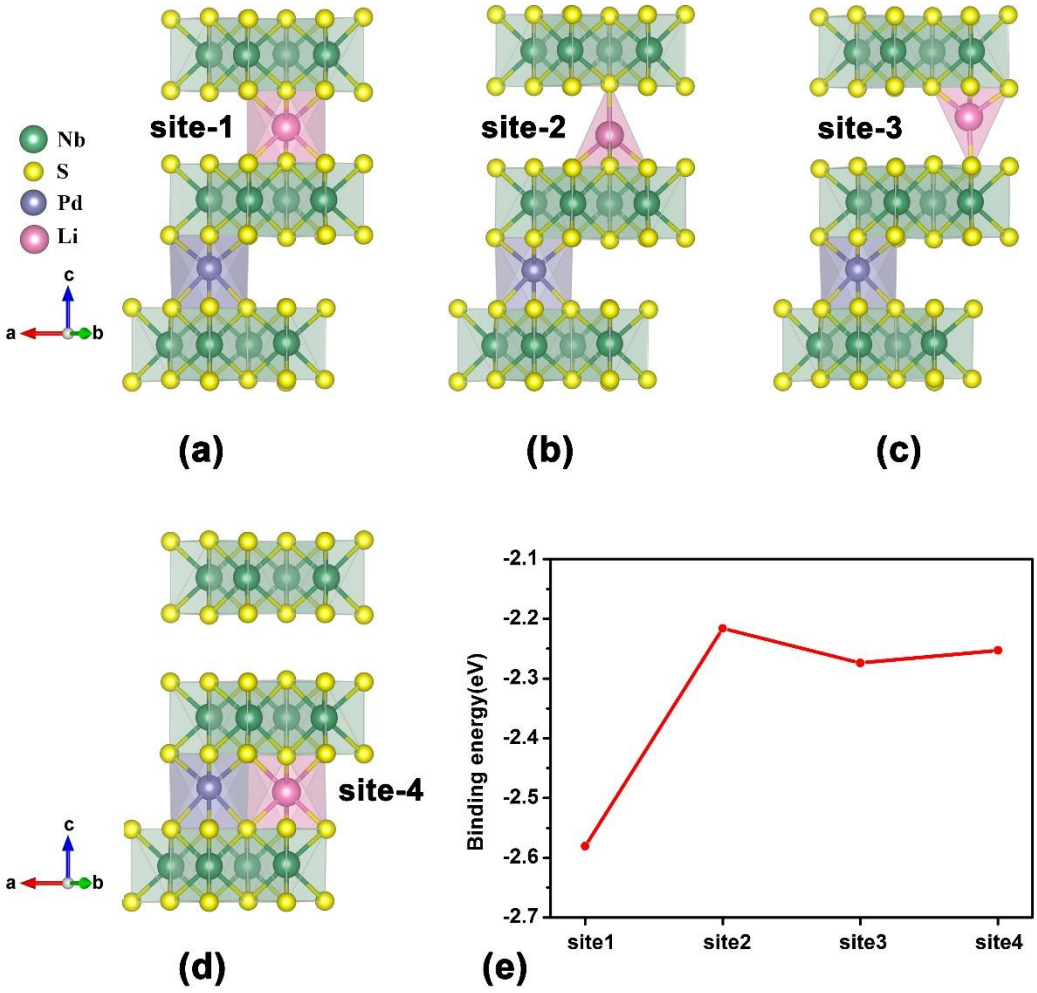

Fig. S13 Schematic diagrams of the Li intercalation positions for the two kinds of octahedral interstice position ((a),(d)) and two kinds of tetrahedral interstice position((b),(c)). (e) The binding energies as a function of positions of Li ions in the $Pd_{0.083}NbS_2$.

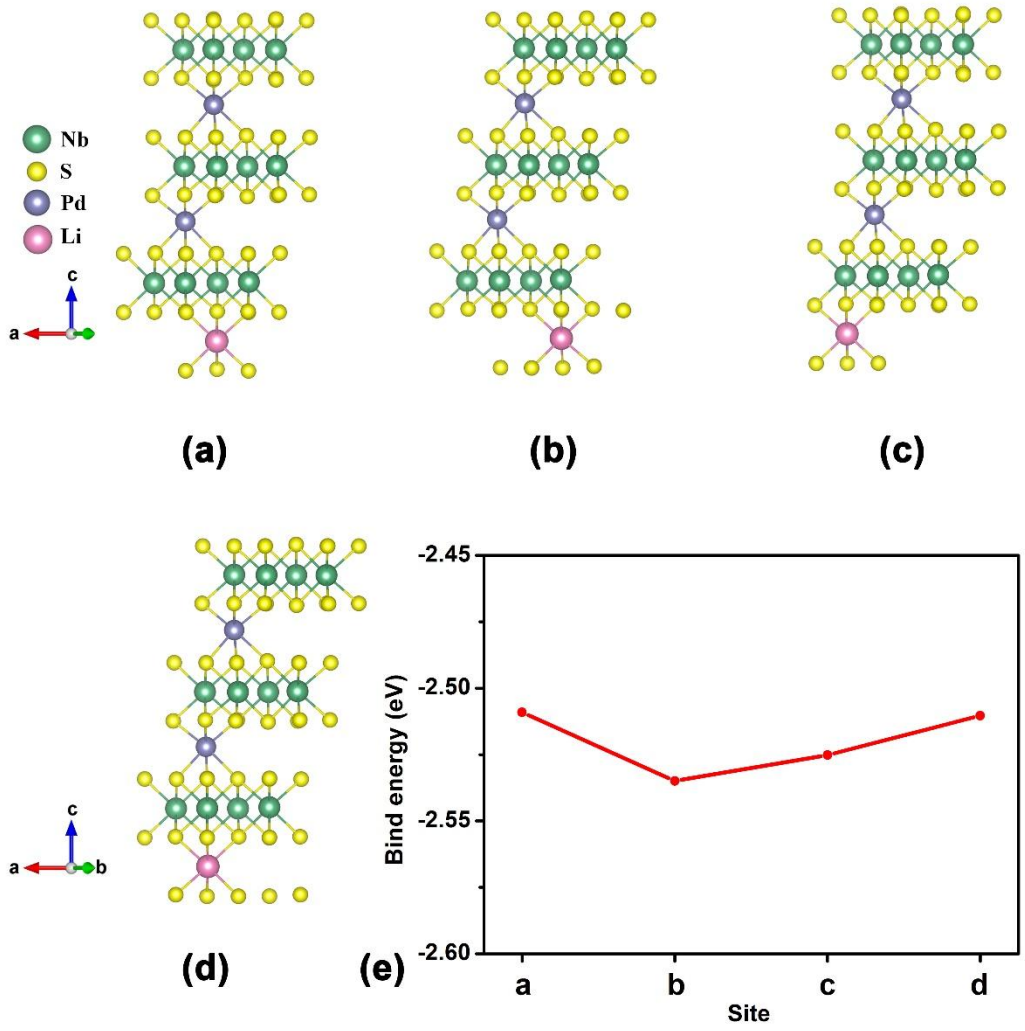

Fig. S14 Schematic diagrams of the Li embedding site in $Pd_{0.167}NbS_2$ ((a)-(d)). (e) And the corresponding binding energies as a function Li embedding site.

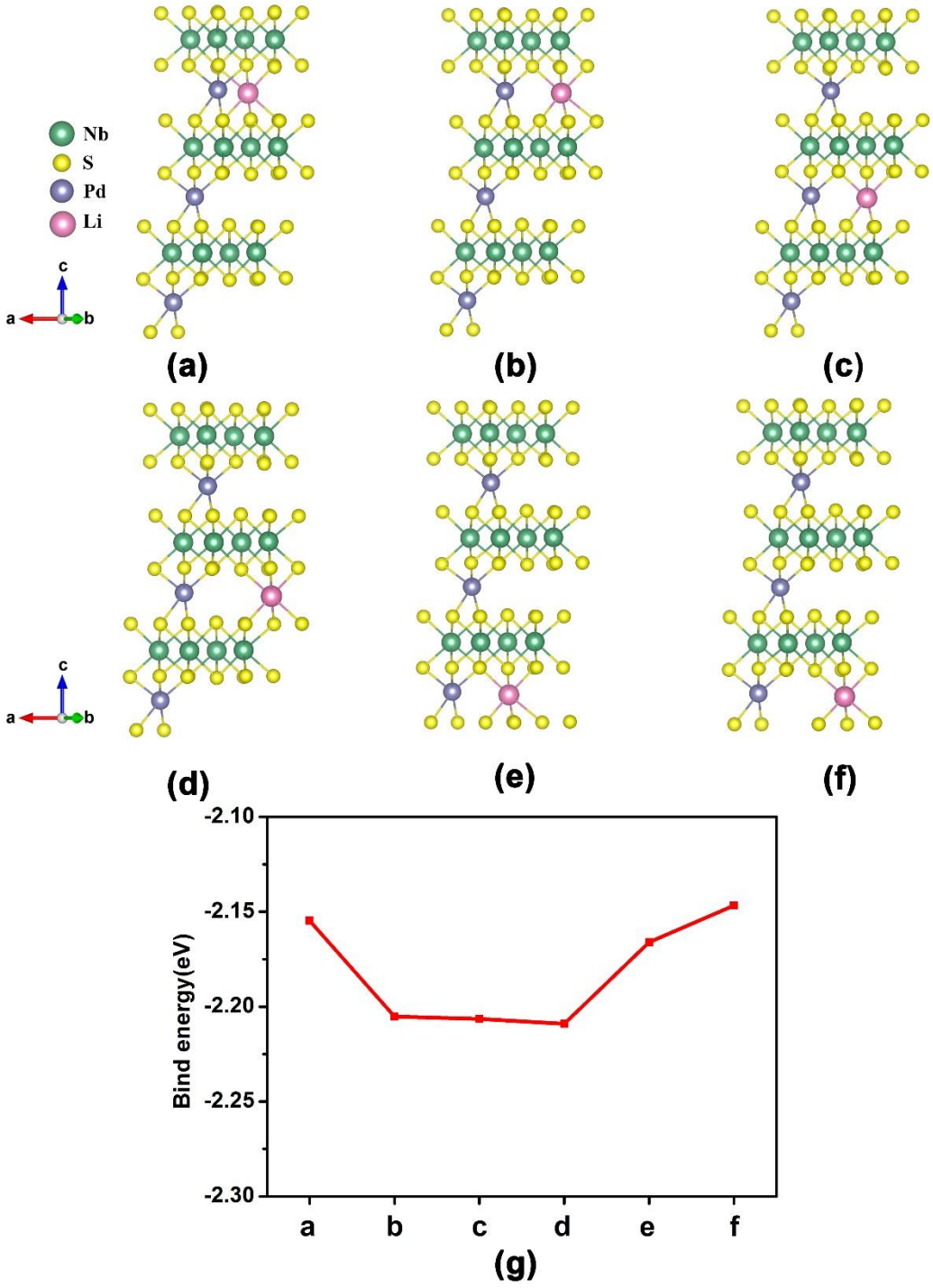

Fig. S15 Schematic diagrams of the Li embedding site of $Pd_{0.25}NbS_2$ ((a)-(f)). (g) And the corresponding binding energies as a function Li embedding site.

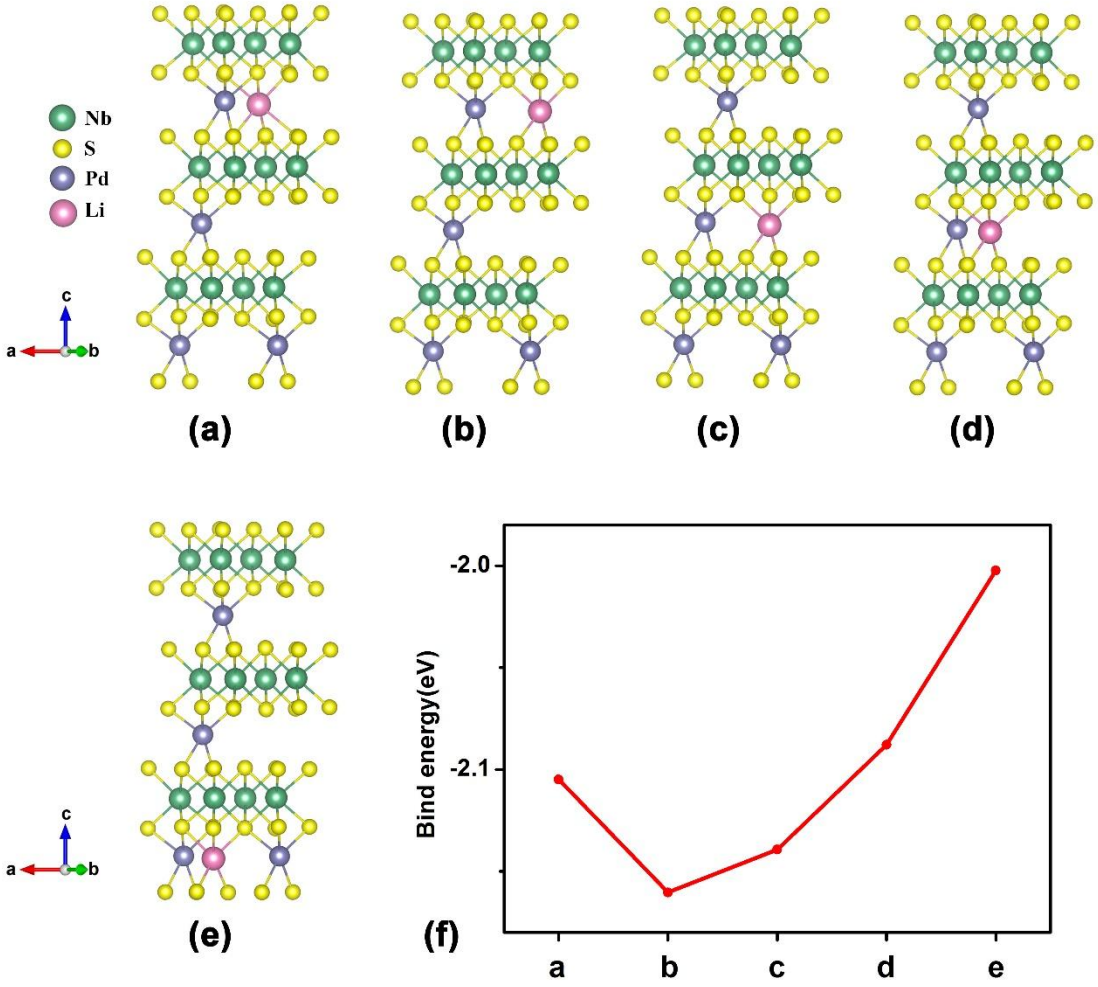

Fig. S16 Schematic diagrams of the Li embedding site of $Pd_{0.333}NbS_2$ ((a)-(e)). (f) And the corresponding binding energies as a function Li embedding site.

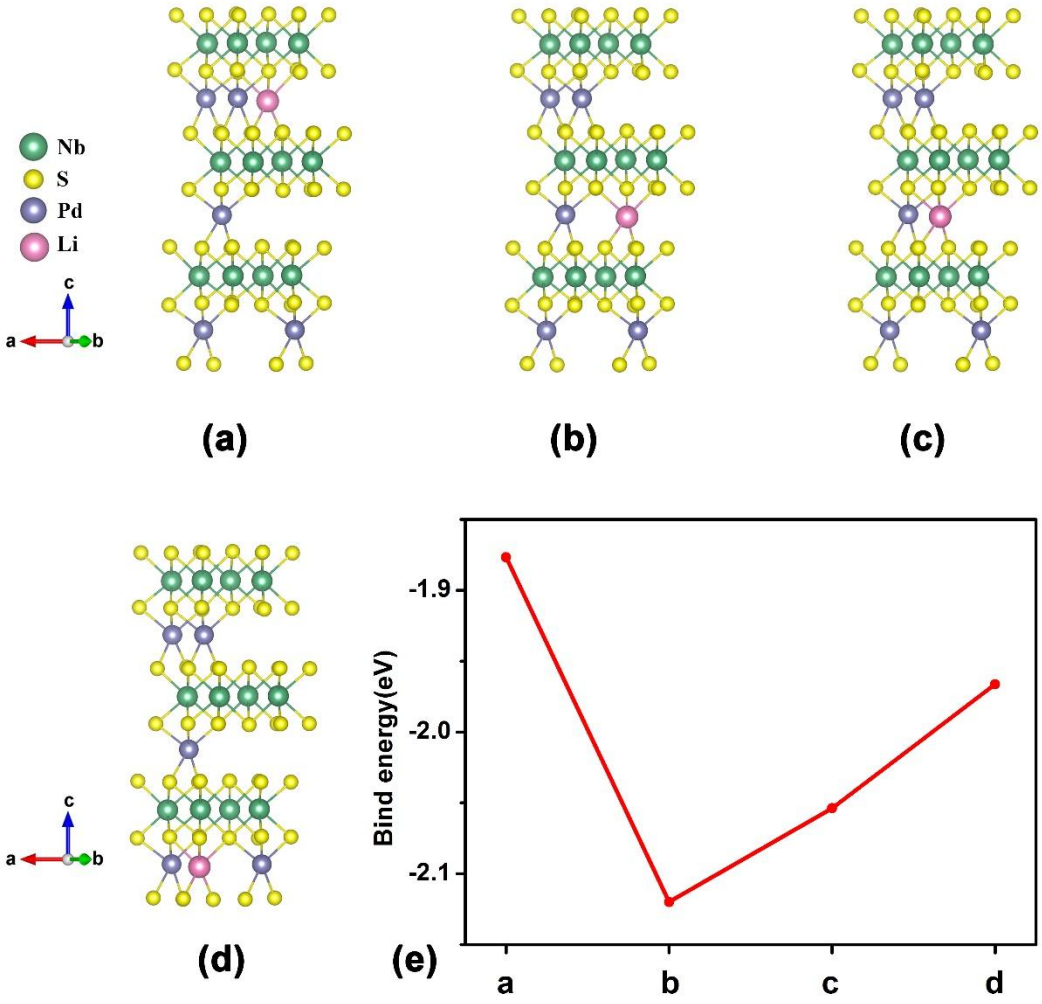

Fig. S17 Schematic diagrams of the Li embedding site of $Pd_{0.417}NbS_2$ ((a)-(d)). (e) And the corresponding binding energies as a function Li embedding site.

5. Migration process of Li-ion in the Pd_xNbS_2 (x = 0, 0.083, 0.167, 0.250, 0.333, 0.417)

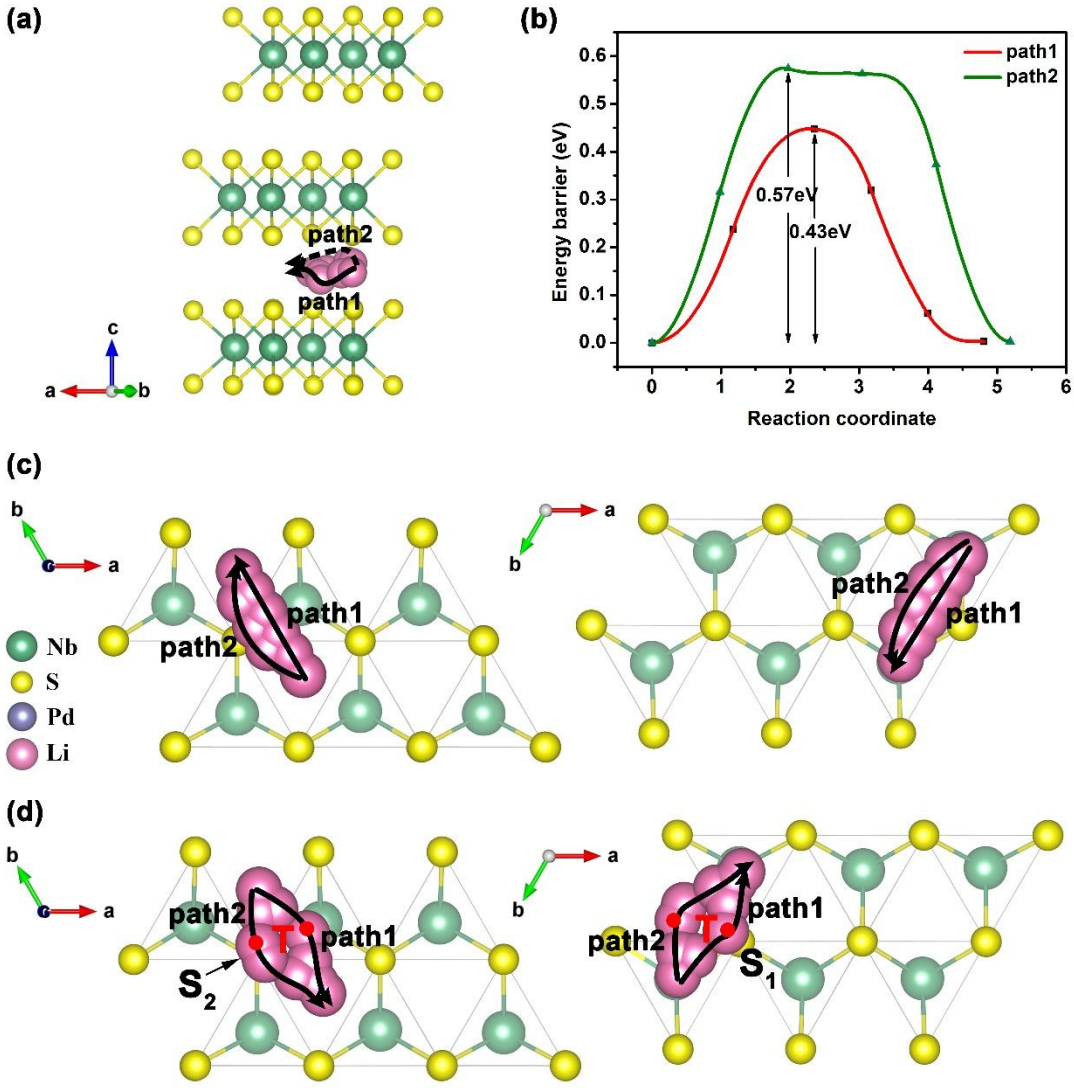

Fig. S18 (a) Two Li-ion diffusion paths and (b) their corresponding diffusion barriers in the NbS_2; Top view of the Li-ion diffusion paths of (c) unrelaxed structure and (d) relaxed structure in the NbS_2.

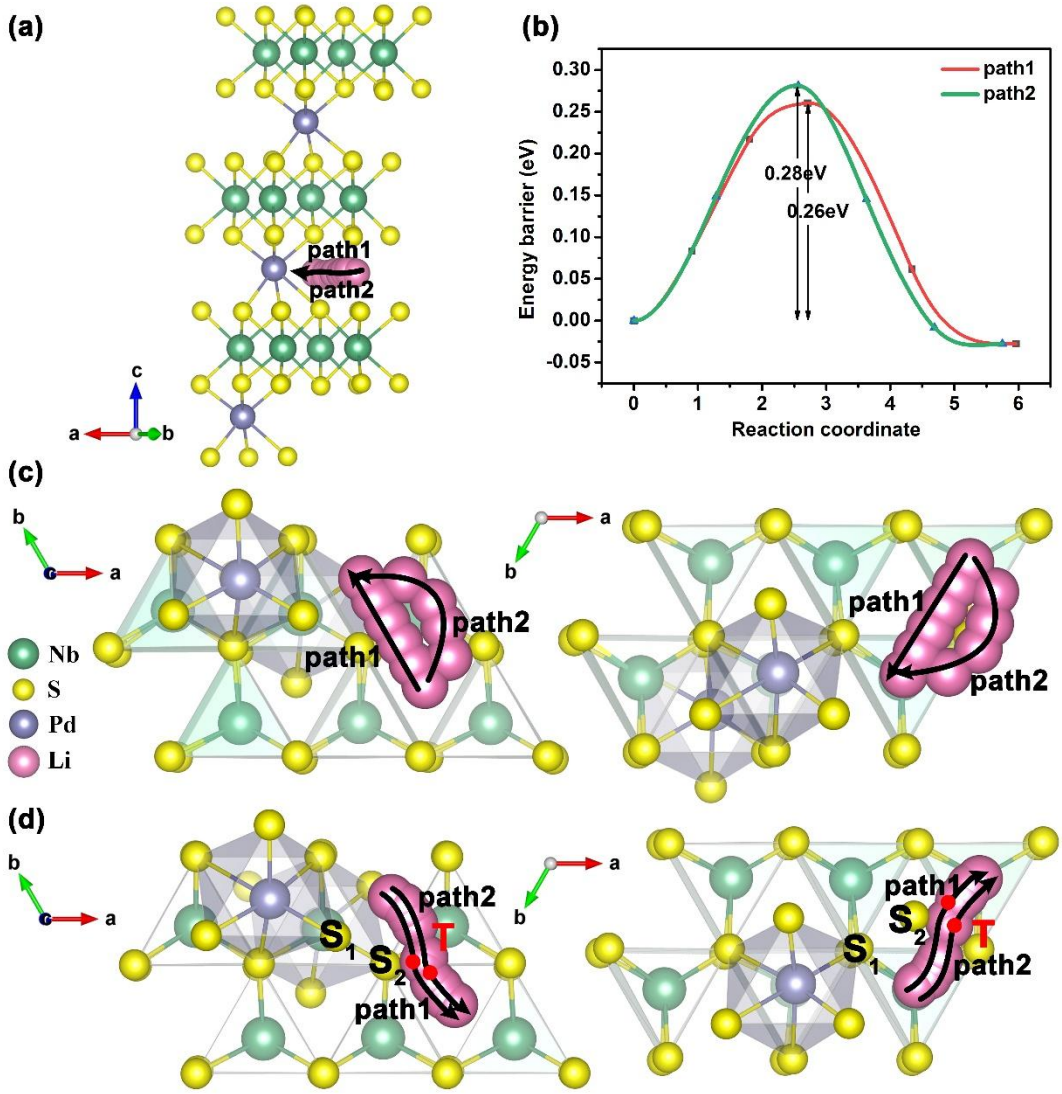

Fig. S19 (a) Two Li-ion diffusion paths and (b) their corresponding diffusion barriers in the $Pd_{0.25}NbS_2$; Top view of the Li-ion diffusion paths of (c) unrelaxed structure and (d) relaxed structure in the NbS_2.

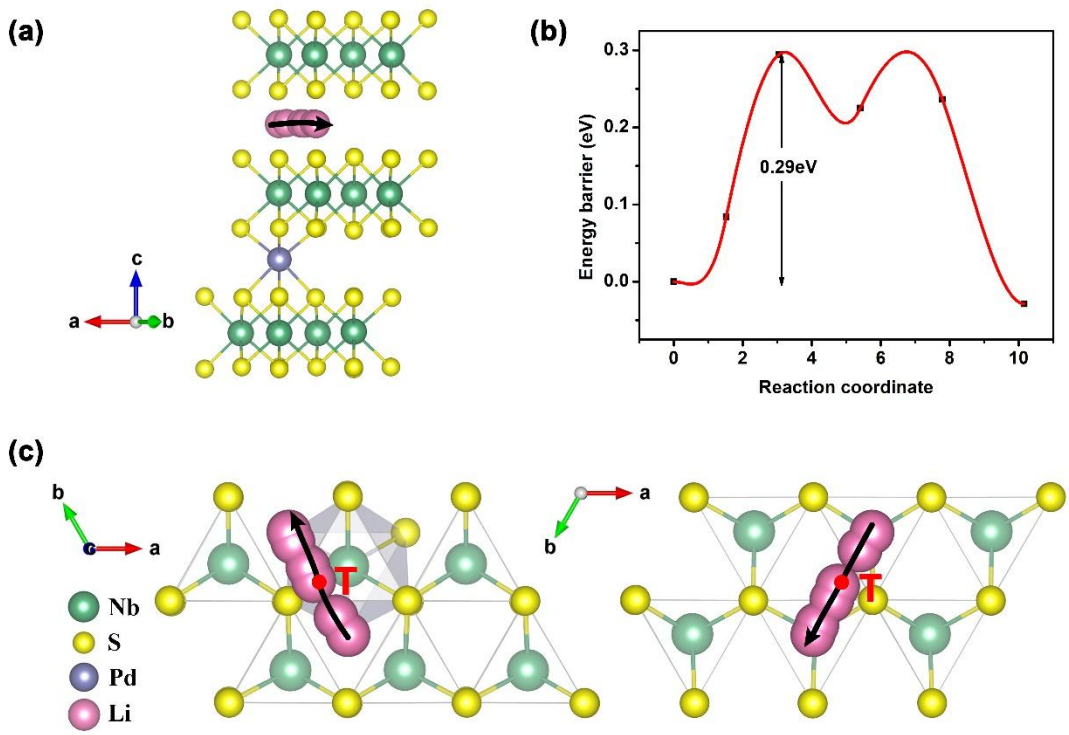

Fig. S20 (a) The favorable Li-ion diffusion path and (b) the corresponding diffusion barrier in the $Pd_{0.083}NbS_2$; (c) Top view of the favorable Li-ion diffusion paths in the $Pd_{0.083}NbS_2$.

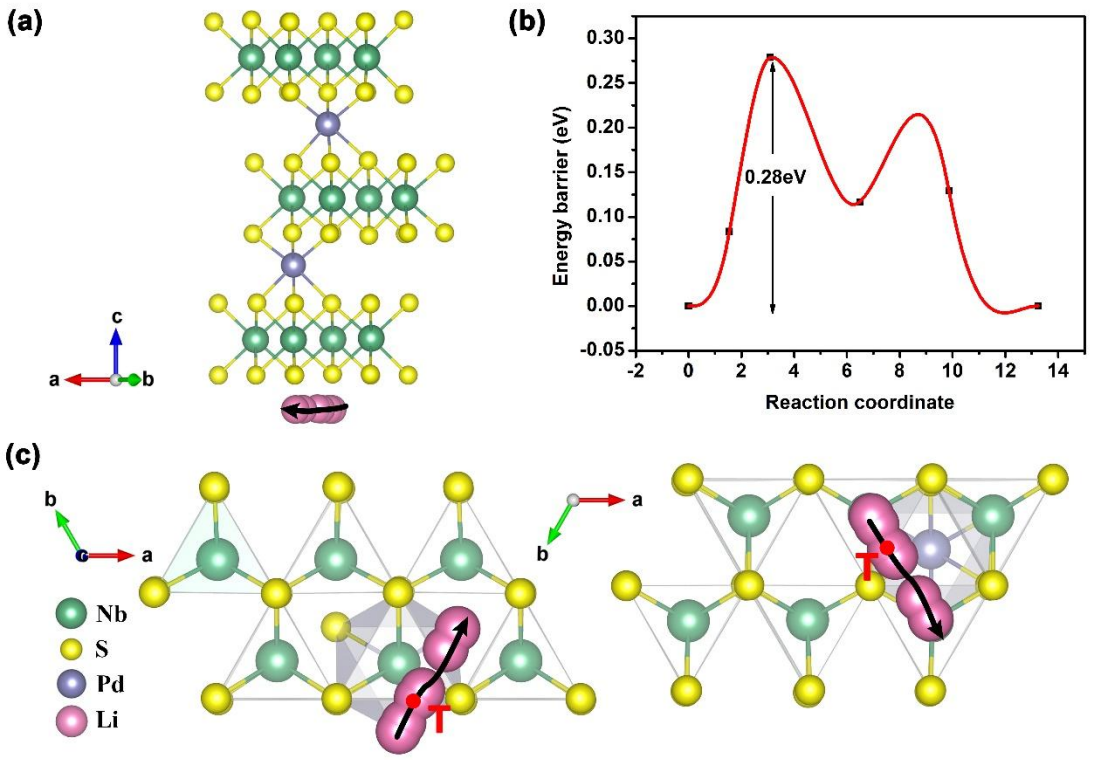

Fig. S21 (a) The favorable Li-ion diffusion path and (b) the corresponding diffusion barrier in the $Pd_{0.167}NbS_2$; (c) Top view of the favorable diffusion paths in the $Pd_{0.167}NbS_2$.

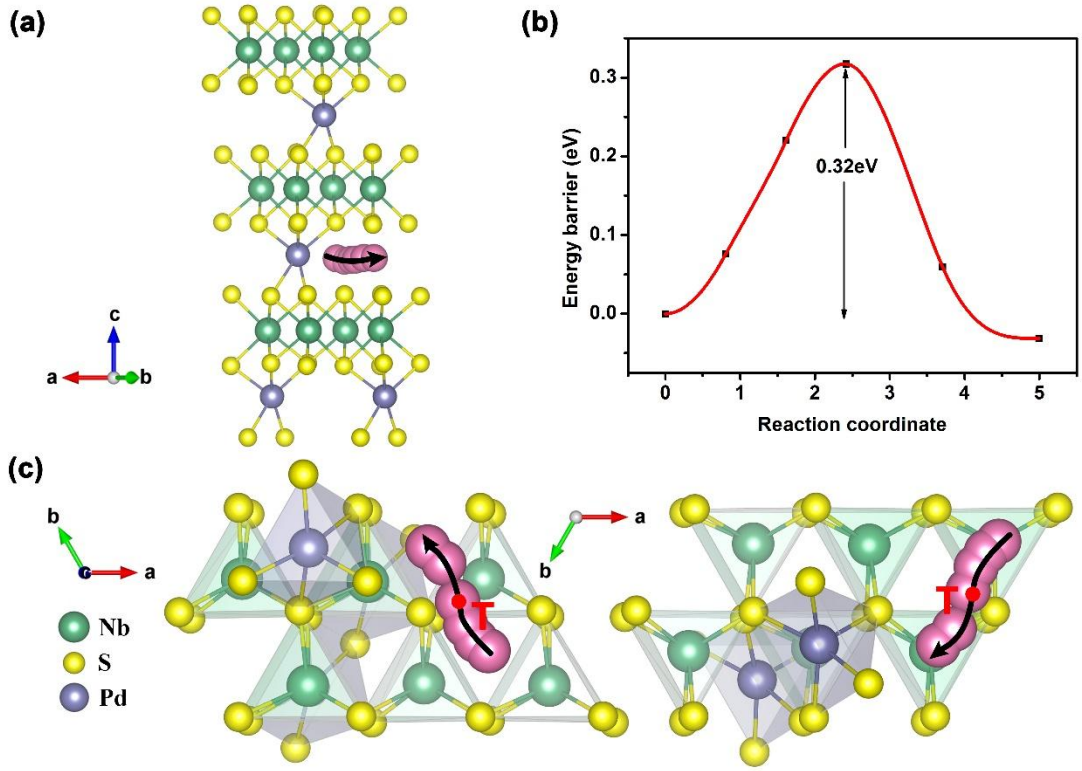

Fig. S22 (a) The favorable Li-ion diffusion path and (b) the corresponding diffusion barrier in the $Pd_{0.333}NbS_2$; (c) Top view of the favorable diffusion paths in the $Pd_{0.333}NbS_2$.

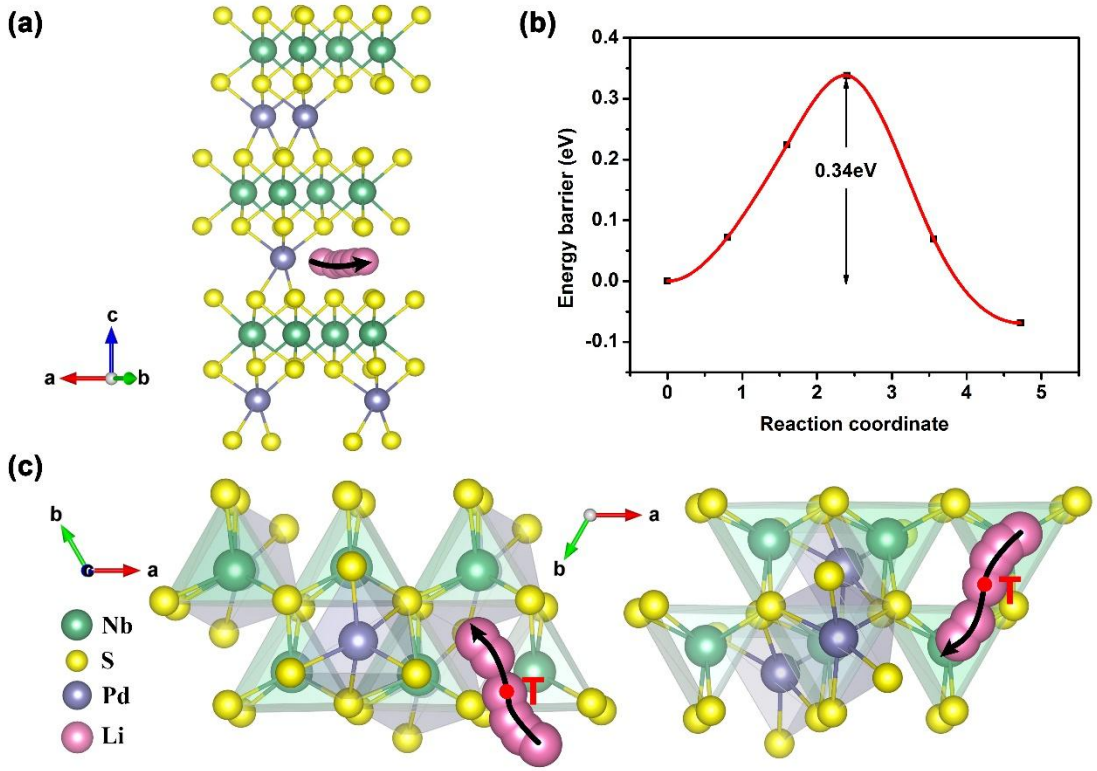

Fig. S23 (a) The favorable Li-ion diffusion path and (b) the corresponding diffusion barrier in the $Pd_{0.417}NbS_2$; (c) Top view of the favorable diffusion paths in the $Pd_{0.417}NbS_2$.

Next, we further analyzed the bonding behavior and PDOS of S1-Li-S2 structure in the transition states of $Pd_{0.25}NbS_2$ and NbS_2. It can be seen from the DOS of Fig. S24(a) and (d) that Li-S orbit and S1&S_2-3p orbit have different degrees of hybridization between -4 eV and 4 eV. Therefore, it can be determined that the bond distance of Li-S interacts with each other stays in the range of 2.19 Å ~ 2.66 Å. Then it is determined that the coordination number of Li-S in initial state of $Pd_{0.25}NbS_2$ and NbS_2 is 6, while Li-S coordination numbers of transition state $Pd_{0.25}NbS_2$ and NbS_2 are 5 and 4, respectively. This will lead to a small energy difference between the initial and transition state structures of Li ions in the diffusion process and then form a

low diffusion energy barrier. Fig. S24(c) and (f) show that charge transfer between Li-ion and, S1 and S2 atoms in the range of 0.09~0.25 eV/Å^2, indicating that there is charge transfer between Li and S.

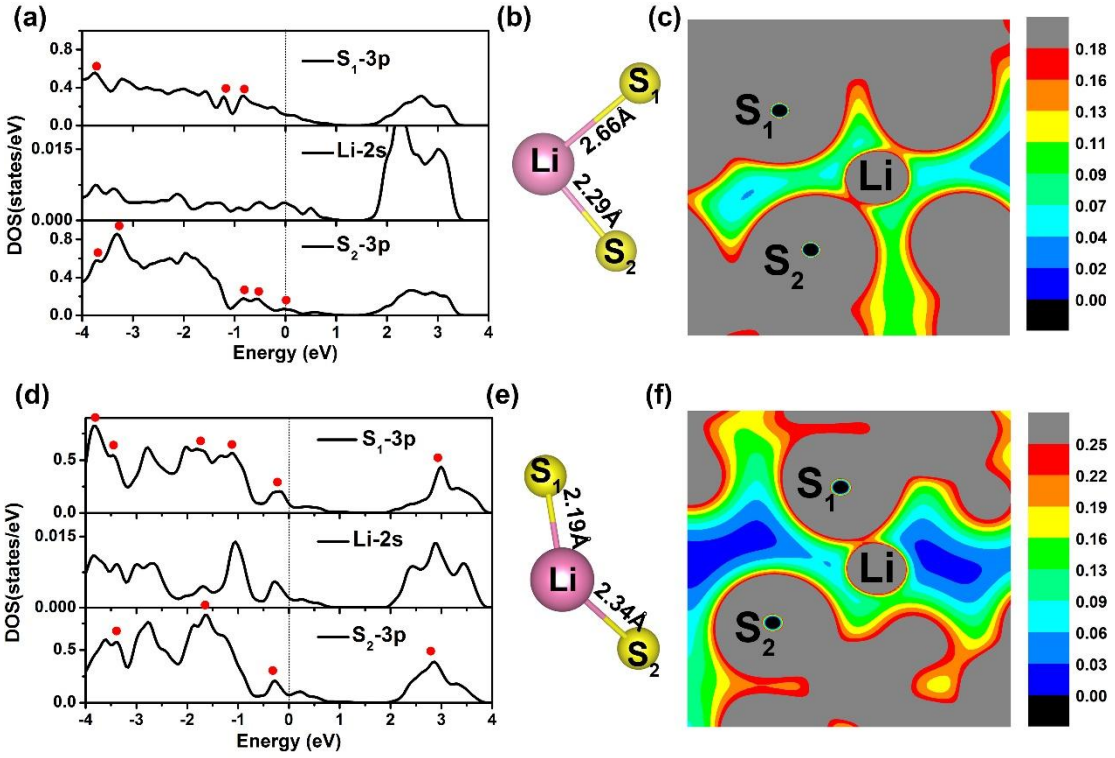

Fig. S24 The partial density of S1-Li-S2 structure in the transition states of (a) $Pd_{0.25}NbS_2$ and (d) NbS_2; Total electron charge densities of S1-Li-S2 structure in the transition states of (c) $Pd_{0.25}NbS_2$ and (f) NbS_2. The S1-Li-S2 structures of (c) $Pd_{0.25}NbS_2$ and (e) NbS_2 of the transition state.

6. Electrochemical performance of Li-ion in the Pd_xNbS_2

The insertion/deinsertion behavior of Li-ions in Pd_xNbS_2 (x = 0, 0.25) follows the voltage chemical reaction equation:

$$Li_{x_1}NbS_2 + (x_2 - x_1) \leftrightarrow Li_{x_2}NbS_2 \quad (2)$$

$$Li_{x_1}Pd_{0.25}NbS_2 + (x_2 - x_1) \leftrightarrow Li_{x_2}Pd_{0.25}NbS_2 \quad (3)$$

The theoretical voltages can be obtained by the following equation:[49]

$$V_{ave} = -\frac{E_{Li_{x_1}NbS_2} - (E_{Li_{x_2}NbS_2} + (x_2 - x_1)E_{Li})}{(x_2 - x_1)e} \quad (4)$$

Where $E_{Li_{x_1}NbS_2}$ ($E_{Li_2NbS_2}$) and E_{Li} are the total energy of Li_xNbS_2 per unit formula and the bulk energy of lithium per atom, respectively. x_1 (x_2) is the number of lithium atoms. Similarly, the theoretical voltage of $Pd_{0.25}NbS_2$ can be obtained based on the equation above.

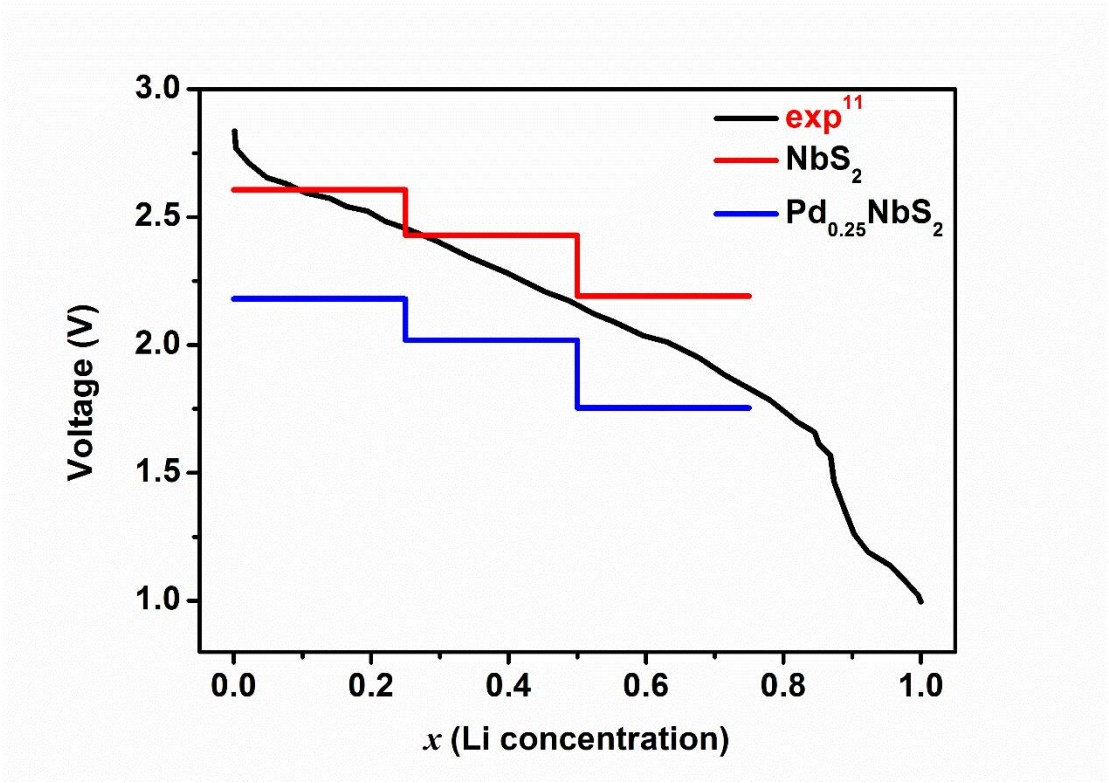

Fig. S25 The theoretical voltage for Li content as a function of specific capacity.

Table S1 The calculated lattice constants of NbS_2 by different vDW correction methods

	EXP	DFT-D2	DFT-D3	optB86b-vdW
a (Å)	3.330	3.341	3.323	3.327
c (Å)	17.918	18.237	17.856	17.949
V(Å^3)	172.100	176.252	170.768	172.286

Table S2 The calculated lattice constants of $Pd_{0.25}NbS_2$ by different vDW correction methods

	DFT-D2	DFT-D3	optB86b-vdW
a (Å)	3.350	3.341	3.347
c (Å)	18.596	18.730	18.768
V(Å^3)	180.119	179.508	180.897

Table S3 Lattice constants of Pd_xNbS_2 (x = 0, 0.083, 0.167, 0.250, 0.333, 0.417)

	a(Å)	b(Å)	c(Å)	α	β	γ	V(Å^3)
NbS_2	6.654	6.654	17.949	90.000°	90.000°	120.000°	688.174
$Pd_{0.083}NbS_2$	6.648	6.648	18.293	90.002°	89.998°	120.000°	700.157
$Pd_{0.167}NbS_2$	6.667	6.667	18.494	90.720°	89.280°	120.101°	711.204
$Pd_{0.250}NbS_2$	6.694	6.694	18.771	92.963°	87.037°	120.447°	723.848
$Pd_{0.333}NbS_2$	6.718	6.718	19.025	94.932°	85.069°	120.710°	734.579
$Pd_{0.417}NbS_2$	6.737	6.729	19.260	96.084°	83.891°	120.898°	743.642

Table S4 The elastic constants of Pd_xNbS_2 (x = 0, 0.083, 0.167, 0.250, 0.333, 0.417)

Elastic constants	***C*11**	***C*12**	***C*13**	***C*14**	***C*33**	***C*44**	***C*66**
NbS_2	136.423	107.417	12.777	38.735	59.792	12.151	14.503
$Pd_{0.083}NbS_2$	140.277	109.393	15.334	39.080	66.584	8.346	15.442
$Pd_{0.167}NbS_2$	141.032	109.669	20.233	39.997	77.468	7.836	15.682
$Pd_{0.250}NbS_2$	138.325	107.925	36.320	39.673	100.262	13.014	15.200
$Pd_{0.333}NbS_2$	142.555	110.455	42.035	39.873	110.000	18.974	16.050
$Pd_{0.417}NbS_2$	143.458	111.052	48.435	39.853	128.402	23.469	16.203

Table S5 The bulk modulus(*B*), shear modulus(*G*), Young's modulus(*E*), Poisson's ratio(*v*) and *B*/*G* of Pd_xNbS_2 (x = 0, 0.083, 0.167, 0.250, 0.333, 0.417).

Samples	***B*(*GPa*)**	***G*(*GPa*)**	***E*(*GPa*)**	**Poisson's ratio（*v*）**	***B*/*G***
EXP	57.000[4]		53.100[5]	0.350[6]	
NbS_2	56.073	18.101	49.026	0.354	3.098
$Pd_{0.083}NbS_2$	59.970	16.444	45.201	0.3744	3.647
$Pd_{0.167}NbS_2$	65.301	16.266	45.057	0.385	4.015
$Pd_{0.250}NbS_2$	77.572	18.796	52.174	0.388	4.127
$Pd_{0.333}NbS_2$	83.798	22.288	61.419	0.378	3.760
$Pd_{0.417}NbS_2$	90.240	24.171	66.568	0.377	3.734

Table S6 The corresponding crystal structure space group and formation enthalpy in the Nb-S system. The reference values in Materials Project and other research are listed.

Phase	**Structure**	**GGA**	**Materials Project**	**Ref**
$Nb_{14}S_5$	Pnma	-13.99	-13.34	-11.59[7]
Nb_3S_4	P63/m	-10.29	-10.35	-9.81[7]
NbS	P63/mmc	-2.53	-2.47	-2.14[7]
NbS_3	P1	-4.86	-5.01	-4.16[7]
$Nb_{21}S_8$	I4/m	-22.21	-21.00	/
NbS_2	R3mh	-4.29	-4.25	-3.72[7]

Table S7 Corresponding crystal structure space group and formation enthalpy in compounds containing Pd. The reference values in Materials Project and other research are listed.

Phase	structure	GGA	Materials Project	Ref
$NbPd_3$	I4/mmm	-1.81	-1.69	-1.74[8]
$Pd_{16}S_7$	I$\bar{4}$3m	-10.30	-9.38	-13.22[9, 10]
Pd_3S	Ama2	-1.52	-1.34	-1.12[9, 11]
Pd_4S	P$\bar{4}$21c	-1.55	-1.42	-1.26[9, 11]
PdS	P42/m	-1.37	-1.24	-1.76[9, 10]
PdS_2	Pbca	-2.13	-1.79	-2.70[10]
Nb_2PdS_5	C2/m	-10.03	-9.43	
Nb_2PdS_6	C2/m	-10.75	-10.11	

Table S8 Constraint conditions of the competitive phase in compounds containing Pd and its corresponding Pd relative chemical potential.

Phase	Constraint conditions	Bounded Value
$NbPd_3$	$\Delta\mu_{\mathrm{Nb}} + 3\Delta\mu_{\mathrm{Pd}} \leq \Delta H_f(\mathrm{NbPd_3})$	$\Delta\mu_{Pd}$ = -0.033
$Pd_{16}S_7$	$16\Delta\mu_{\mathrm{Pd}} + 7\Delta\mu_{\mathrm{S}} \leq \Delta H_f(\mathrm{Pd_{16}S_7})$	$\Delta\mu_{Pd}$ = -0.336
Pd_3S	$3\Delta\mu_{\mathrm{Pd}} + \Delta\mu_{\mathrm{S}} \leq \Delta H_f(\mathrm{Pd_3S})$	$\Delta\mu_{Pd}$ = -0.256
Pd_4S	$4\Delta\mu_{\mathrm{Pd}} + \Delta\mu_{\mathrm{S}} \leq \Delta H_f(\mathrm{Pd_4S})$	$\Delta\mu_{Pd}$ = -0.211
PdS	$\Delta\mu_{\mathrm{Pd}} + \Delta\mu_{\mathrm{S}} \leq \Delta H_f(\mathrm{PdS})$	$\Delta\mu_{Pd}$ = -0.668
PdS_2	$\Delta\mu_{\mathrm{Pd}} + 2\Delta\mu_{\mathrm{S}} \leq \Delta H_f(\mathrm{PdS_2})$	$\Delta\mu_{Pd}$ = -0.645
Nb_2PdS_5	$2\Delta\mu_{\mathrm{Nb}} + \Delta\mu_{\mathrm{Pd}} + 5\Delta\mu_{\mathrm{S}} \leq \Delta H_f(\mathrm{Nb_2PdS_5})$	$\Delta\mu_{Pd}$ = -3.745
Nb_2PdS_6	$2\Delta\mu_{\mathrm{Nb}} + \Delta\mu_{\mathrm{Pd}} + 6\Delta\mu_{\mathrm{S}} \leq \Delta H_f(\mathrm{Nb_2PdS_6})$	$\Delta\mu_{Pd}$ = -3.895

References:

1. Z. Zhu, I.-H. Chu, Z. Deng and S. P. Ong, *Chemistry of Materials*, 2015, **27**, 8318-8325.
2. Q. Peng, Z. Wang, B. Sa, B. Wu and Z. Sun, *ACS Appl Mater Interfaces*, 2016, **8**, 13449-13457.
3. M. Chi and Y.-P. Zhao, *Computational Materials Science*, 2009, **46**, 1085-1090.
4. W. Wang, W. Lei, X. Zheng, H. Li, X. Tang and X. Ming, *Chinese Physics B*, 2020, **29**.
5. P. Malchow, K. E. Johanns, D. Möncke, S. Korte-Kerzel, L. Wondraczek and K. Durst, *Journal of Non-Crystalline Solids*, 2015, **419**, 97-109.
6. Y. Zang, Y. Ma, R. Peng, H. Wang, B. Huang and Y. Dai, *Nano Research*, 2020, **14**, 834-839.
7. R. Lucrezi and C. Heil, *J Phys Condens Matter*, 2021, **33**.
8. D. A. Carr, J. Corbitt, G. R. Hart, E. Gilmartin and G. L. W. Hart, *Computational Materials Science*, 2012, **51**, 331-339.
9. R. Hu, M. C. Gao, Ö. N. Doğan, P. King and M. Widom, *Calphad*, 2010, **34**, 324-331.
10. M. Stickney, M. Chandrasekharaiah, K. Gingerich and J. Speed, *Metallurgical Transactions A*, 1991, **22**, 1937-1943.
11. W. P. Huhn, M. Widom and M. C. Gao, *Computational Materials Science*, 2014, **92**, 377-386.